

Received July 26, 2019, accepted August 6, 2019, date of publication August 19, 2019, date of current version November 19, 2019.

Digital Object Identifier 10.1109/ACCESS.2019.2936256

Active Modeling and Control for Shape Memory Alloy Actuators

DAOHUI ZHANG^{ID1,2}, XINGANG ZHAO^{ID1,2}, (Member, IEEE), JIANDA HAN^{ID3}, (Member, IEEE),
XIAOGUANG LI^{1,2,4}, AND BI ZHANG^{ID1,2}

¹State Key Laboratory of Robotics, Shenyang Institute of Automation, Chinese Academy of Sciences, Shenyang 110016, China

²Institutes for Robotics and Intelligent Manufacturing, Chinese Academy of Sciences, Shenyang 110016, China

³College of Computer and Control Engineering, Nankai University, Tianjin 300350, China

⁴School of Chemical Equipment, Shenyang University of Technology, Shenyang 110870, China

Corresponding author: Jianda Han (hanjianda@nankai.edu.cn)

This work was supported by the National Natural Science Foundation of China under Grant 61903360, Grant 61773369, and Grant U1813214.

ABSTRACT In this paper, an active modeling and control scheme is developed for Shape Memory Alloy (SMA) actuators to eliminate the negative influences caused by the uncertainties in its dynamics. First, a nonlinear SMA dynamic model based on Liang model and the empirical models is built and linearized, and all the uncertainties due to time-varying parameters, external disturbances, as well as the linearization, are considered as model error of the linearized model. Secondly, an active modeling based on Kalman filter is constructed to estimate the model error in real time, which intends to improve the model accuracy actively. Finally, an active modeling based control method is proposed to compensate the model error in order to improve control performance of SMA actuators. Experiments are conducted on a one degree-of-freedom (DOF) testbed actuated by a SMA wire. The experimental results of the active model error estimation, and the control performance with and without the active model based compensation are presented and compared to demonstrate the improvements of the proposed scheme.

INDEX TERMS Shape memory alloy (SMA), model error, active modeling, active compensation control.

I. INTRODUCTION

The shape memory alloy (SMA) wire can decrease in actuating length through a resistive heating from an electrical current due to a crystalline phase transformation from martensite (the low temperature phase) to austenite (the high temperature phase) [1]. Compared to conventional motors, hydraulic actuators, gas cylinders, and new nano-actuators [2], [3], SMA actuators have intrinsic compliance, large force-to-mass ratio, biocompatibility, compact size, light weight, and quiet operation that makes it feasible for soft robotics, exoskeletal robotics, and biomimetic robotics [4]–[8]. However, the phase transformation dynamics of SMA involves nonlinearity, hysteresis and time-varying parameters, which make it difficult to design high-performance controllers [9], [10]. Generally, there are two ways to improve the performance of a SMA actuator, namely: 1) trying to construct a more accurate model that meets the SMA dynamics

in all of its working conditions; and 2) designing a controller that could reject the modeling errors well.

Currently, there are three main types of models that have been proposed to describe the SMA dynamics, namely, the phenomenological model, the physical model, and the neural network (NN) based model. The phenomenological models, such as Preisach model [11], [12], Krasnoselskii-Pokrovskii model [13], Prandtl-Ishlinskii model [14], etc., describe the hysteresis by a collection of weighted elementary functions. The complex and generally multidimensional structure of this method makes it difficult to tune the parameters in real time to meet the change of the operating environment of SMA actuators [15], [16]. The physical models, on the other hand, including Duhem model [17], Bouc-Wen model [18], Liang model [19], [20], and other empirical models [21], [22], describe the SMA behavior based on its physical properties. However, the parameters inside the physical models are usually identified offline, which may lead to large modeling error while the SMA actually working in a condition different from that the model were identified. Multilayer neural network [23], hysteretic recurrent neural

The associate editor coordinating the review of this manuscript and approving it for publication was Hamid Mohammad-Sedighi.

network [24], [25], neuro-fuzzy network [26], etc., are also proposed to model SMA dynamics. The main difficulty of this NN-based way is how to acquire an ‘enough’ dataset to train the neural network offline so that the model could present good performance in all of the working conditions of SMA actuators.

Besides the proposed models, control schemes were also studied in order to improve the performance of SMA actuators. A self-tuning fuzzy PID controller was applied to compensate the SMA hysteresis phenomena [27]. Slide mode control (SMC) was utilized to reject the model uncertainties. Fuzzy logic [28] and neural network [25], [29] enhanced SMC were further proposed to avoid the frequent mode switches, which might excite the resonance vibrations of SMA actuators. Adaptive control algorithms, such as output feedback direct adaptive control [30], model reference active control [31], and robust indirect adaptive control [32], etc., were proposed to control SMA actuators. Moreover, neural network model predictive control [33], neural network feed-forward control with RISE feedback [34] and neural network direct control with online learning [35] were also used to control the modeling error of SMA actuators. However, how to reject the modeling error effectively in a wide working condition of SMA actuators is still an open problem.

In this paper, we proposed a new active control scheme for SMA actuators. The proposed scheme consists of a feedback linearization for nonlinear SMA dynamics, an active estimator for joint estimation, and a compensation controller for high precision tracking. Here, we use some existing algorithms, e.g. Kalman filter and state feedback control, which have low computational burden and are easily implemented on real system, to construct and verify the new active scheme. Indeed, these existing algorithms themselves do not have some special new and they are not the focus of this paper as well. However, the constructed active control scheme, rather than these existing algorithms themselves, is actually the main contribution of our work, and it is the first of its kind to be evaluated through experimental trials involving SMA actuators. In order to demonstrate the effectiveness of the proposed scheme, control experiments with and without active model based compensation were conducted and compared on a one-DOF testbed actuated by a SMA wire. Experimental results show, compared to conventional state feedback control, the proposed control demonstrates significant improvement under different frequency trajectories and different loads.

The rest of this paper is organized as follows: Section II introduces the nonlinear model of SMA as pre-knowledge. Then, the proposed active modeling and control techniques are presented in Section III, followed by the experimental studies and comparisons in Section IV. Finally, Section V draws the conclusion.

II. PRE-KNOWLEDGE: NONLINEAR MODEL OF SMA

As mentioned above, many SMA models have been proposed, and we have summarized them into tree categories.

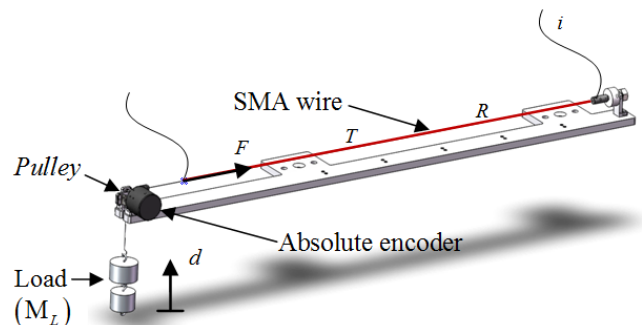


FIGURE 1. A typical SMA actuated system.

The focus of this paper is to propose an active modeling approach, which can be built on an existing model. The model developed in this work is based on Liang model [19], [20] and the empirical models [21], [22]. Thus, here we only briefly describe the modeling process of SMA.

Fig. 1 shows the typical structure of a SMA actuated mechanism, where: F is the force acting on the SMA wire; d is the displacement of the load; and M_L is the mass of the load; i is the electric current applied to the SMA wire; R is the electrical resistance per unity length of the wire; T is the wire temperature. By using a linear spring analogy, The traction of the SMA wire is given by $F = K(\xi)(\Delta - d)$, where $K(\xi)$ is the stiffness of the wire, ξ is the martensite fraction; $\Delta = 0.04l_{wire}$, and l_{wire} is the maximum length of the SMA wire in martensite phase. By the use of the basic laws of mechanics, the dynamics of the system can be described as [19]:

$$I\ddot{d} + c\dot{d} + K(\xi)d = -M_Lg + K(\xi)\Delta \quad (1)$$

where the inertia item is defined as $I = (J/r^2 + M_L)$, J is the moment of inertia, r is the radius of the pulley; c is the damping coefficient; and g is the gravitational acceleration.

A. WIRE TEMPERATURE T

The heat transfer process, which consists of electrical heating and nature convection, is formulated as [10]:

$$mc_p \frac{dT}{dt} = i^2R - h_cA(T - T_{amb}) \quad (2)$$

where T is the wire temperature; m is the mass per unit length; c_p is the specific heat of the wire; i is the electric current applied to the wire; R is the electrical resistance per unity length; h_c is the heat convection coefficient; A is external area per unity length; and T_{amb} is the ambient temperature.

B. MARTENSITE FRACTION ξ

To eliminate the jump of the martensite fraction during the switches between heating and cooling processes, the

martensite fraction ξ can be modified and given as [36]:

$$\dot{\xi} = \begin{cases} \frac{\xi_M}{1 + \exp\left[\frac{6.2}{A_f - A_s}\left(T - \frac{A_f + A_s}{2}\right)\right]} + k_M, & \dot{T} > 0 \\ \frac{1 - \xi_A}{1 + \exp\left[\frac{6.2}{M_s - M_f}\left(T - \frac{M_f + M_s}{2}\right)\right]} + k_A, & \dot{T} < 0 \end{cases} \quad (3)$$

where

$$\begin{aligned} k_M &= \xi_M - \frac{\xi_M}{1 + \exp\left[\frac{6.2}{A_f - A_s}\left(T_t - \frac{A_f + A_s}{2}\right)\right]}, \\ k_A &= \xi_A - \frac{1 - \xi_A}{1 + \exp\left[\frac{6.2}{M_s - M_f}\left(T_t - \frac{M_f + M_s}{2}\right)\right]}; \end{aligned}$$

ξ_M and ξ_A are the initial martensite fraction during heating and cooling, respectively; A_s and A_f are the initial and final temperature of austenite transformation, respectively; M_s and M_f are the initial and final temperature of martensite transformation, respectively; and T_t is the wire temperature at the switch point.

C. STIFFNESS $K(\xi)$

Due to elastic phenomenon, the stress-strain relationship of the SMA wire can be presented as [22]:

$$\sigma = [\xi E_M + (1 - \xi) E_A] \varepsilon$$

or

$$\frac{F}{A_{\text{wire}}} = [\xi E_M + (1 - \xi) E_A] \frac{\Delta l}{l_0} \quad (4)$$

Then the wire stiffness can be obtained:

$$K(\xi) = [(1 - \xi) E_A + \xi E_M] \frac{A_{\text{wire}}}{l_0} \quad (5)$$

where σ and ε are the stress and strain of the SMA wire, respectively; E_M and E_A are the martensite and austenite Young's Modulus, respectively; A_{wire} is the cross-sectional area of the wire; Δl is the elongation of the wire, and l_0 is the length of the wire in the austenite phase.

III. ACTIVE MODELING AND CONTROL FOR SMA

Due to the complexity of the SMA dynamics like (1-5), it is difficult to obtain an accurate model that could describe the SMA behavior in high fidelity. In order to reject the uncertainties involved in the SMA model, we propose the active modeling and also the relative control techniques in this paper. Shown as Fig. 2, the scheme consists of three main techniques, namely, feedback linearization, active modeling, and outer-loop controller.

A. FEEDBACK LINEARIZATION OF SMA DYNAMICS

According to (1-5), the SMA dynamics can be rewritten as

$$\dot{x} = a(x) + b(x) u \quad (6)$$

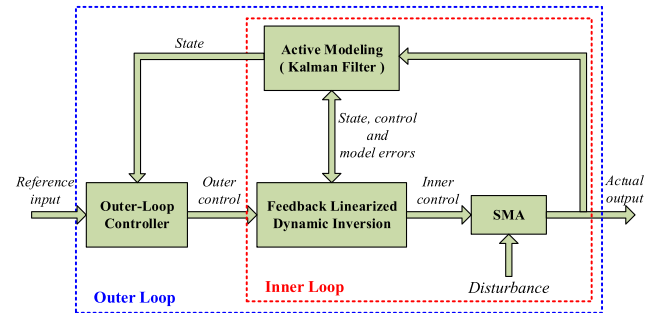


FIGURE 2. Structure of the active modeling and control scheme.

where

$$\begin{aligned} a(x) &= \begin{bmatrix} A_1 x_1 \\ x_3 \\ -\frac{c}{I} x_3 - \frac{K(\xi)}{I} x_2 + \frac{K(\xi)}{I} \Delta - \frac{M_L g}{I} \end{bmatrix}, \\ b(x) &= \begin{bmatrix} B_1 \\ 0 \\ 0 \end{bmatrix}, \quad A_1 = -\frac{h_c A}{mc_p}, \quad B_1 = \frac{R}{mc_p}. \end{aligned}$$

The state vector x and control u are respectively defined as $x = (x_1 \ x_2 \ x_3)^T = (T - T_{\text{amb}} \ d \ \dot{d})^T \in \mathbb{R}^3$, $u = i^2 \in \mathbb{R}$. The nonlinearities in the SMA dynamics mainly exist in $a(x)$, especially $K(\xi)$ involving (2-5) contains strong nonlinearity and hysteresis.

The output function of the system is given by:

$$y = c(x) = x_2 \quad (7)$$

According to [37], the SMA dynamics of (6) can be feedback linearized if and only if $c(x)$ satisfies

$$L_b c(x) = 0, \quad L_b L_a c(x) = 0, \quad L_b L_a^2 c(x) \neq 0 \quad (8)$$

where $L_b c(x) = \frac{\partial c}{\partial x} b(x)$ is called the *Lie Derivative* of c with respect to b or along b .

When satisfying the constraints $\xi_M \neq 0 \cap \xi_A \neq 1 \cap x_2 \neq \Delta$, the linearized state-space equation be given as

$$\begin{cases} \dot{Z}(t) = A_c Z(t) + B_c v \\ Y(t) = C_c Z(t) \end{cases} \quad (9)$$

where

$$\begin{aligned} A_c &= \begin{pmatrix} 0 & 1 & 1 \\ 0 & 0 & 1 \\ 0 & 0 & 0 \end{pmatrix}, \quad B_c = \begin{pmatrix} 0 \\ 0 \\ 1 \end{pmatrix}, \\ C_c &= \begin{pmatrix} 1 & 0 & 0 \\ 0 & 1 & 0 \\ 0 & 0 & 1 \end{pmatrix}. \end{aligned}$$

The state vector $Z(t)$, output vector $Y(t)$, and control v are respectively defined as follow:

$$\begin{aligned} Z(t) &= (z_1 \ z_2 \ z_3)^T = (x_2 \ x_3 \ \dot{x}_3)^T \in \mathbb{R}^3; \\ Y(t) &= (x_2 \ x_3 \ \dot{x}_3)^T \in \mathbb{R}^3; \\ v &= \gamma(x) [u - \alpha(x)] \in \mathbb{R}, \end{aligned}$$

with

$$\alpha(\mathbf{x}) = -\frac{L_a^3 c(\mathbf{x})}{L_b L_a^2 c(\mathbf{x})}, \quad \gamma(\mathbf{x}) = L_b L_a^2 c(\mathbf{x}).$$

B. ACTIVE ESTIMATION OF MODELING ERRORS

Let $f(t)$ present all of the modeling errors of (9), including the disturbances, unmodeled uncertainties, as well as those caused by the linearization, then we can describe the modeling errors as [38], [39]:

$$\begin{cases} B_f f(t) = \dot{\tilde{Z}}(t) - \dot{Z}(t) + W(t) \\ \dot{f}(t) = h(t) \end{cases} \quad (10)$$

where $f(t) = [f_1 \ f_2 \ f_3]^T \in \mathbb{R}^3$ represents the modeling errors, and f_1, f_2 and f_3 are the errors with respect to position, velocity, and acceleration respectively; $B_f \in \mathbb{R}^{3 \times 3}$ is a parameter matrix; $Z(t) \in \mathbb{R}^3$ is the model state of (9); $\tilde{Z}(t) \in \mathbb{R}^3$ is the real state of the SMA system; $W(t) \in \mathbb{R}^3$ is the process noise; and $h(t) \in \mathbb{R}^3$ is the process noises that actuate the modeling errors.

According to (9) and (10), the actual dynamics of the SMA actuated system can be represented as

$$\begin{cases} \dot{\tilde{Z}}(t) = A_c Z(t) + B_c v + B_f f(t) + W(t) \\ \dot{f}(t) = h(t) \\ \tilde{Y}(t) = C_c \tilde{Z}(t) + V(t) \end{cases} \quad (11)$$

where $\tilde{Y}(t) \in \mathbb{R}^3$ is the output of the actual system, and $V(t) \in \mathbb{R}^3$ is the measurement noise. Based on the state after modeling error compensation and the measurement noise, the third relation of (11), namely the output function, was obtained to more accurately describe the dynamic behavior of the system.

In order to estimate the state $Z(t)$ and the modeling errors $f(t)$ simultaneously, we propose to use the “joint estimation” technique. To do this, we need to define the extended state as

$$Z_k^a = (\tilde{Z}_k^T \ f_k^T)^T$$

where \tilde{Z}_k , f_k are the sampling values of $\tilde{Z}(t)$ and $f(t)$ at time k , respectively; and the superscript a indicates ‘extended’.

Thus, the discrete equation of (11) can be obtained as

$$\begin{cases} Z_{k+1}^a = A_d^a Z_k^a + B_d^a v_k + W_k^a \\ Y_k = C_d^a Z_k^a + V_k \end{cases} \quad (12)$$

where $A_d^a = \begin{pmatrix} A_d & B_{fd} \\ 0_{3 \times 3} & I_{3 \times 3} \end{pmatrix}$; $B_d^a = \begin{pmatrix} B_d \\ 0_{3 \times 1} \end{pmatrix}$; $W_k^a = \begin{pmatrix} W_k \\ h_k \end{pmatrix}$; $C_d^a = (C_d \ 0_{3 \times 3})$; $B_{fd} = T_s B_f$, and T_s is the sampling time; $0_{m \times n}$ is an $m \times n$ zero matrix; $I_{m \times n}$ is an $m \times n$ unit matrix; $\{A_d, B_d, C_d\}$ is the discrete expression of $\{A_c, B_c, C_c\}$; v_k , Y_k , and V_k are the sampling values of v , $\tilde{Y}(t)$, and $V(t)$, respectively.

Then, we propose to use Kalman filter to estimate in real-time the extended state Z_k^a while using (12) as the reference model. The estimation process includes two steps: 1) predict

the extended state $\hat{Z}_{k+1|k}^a$ and the covariance matrix $P_{k+1|k}$ by using the state-space equation of (12); and 2) update the gain matrix K_k , the extended state $\hat{Z}_{k|k}^a$ and the covariance matrix $P_{k|k}$ by the measurement output Y_k . Finally, we can build the Kalman filter as follow:

$$\begin{cases} \hat{Z}_{k+1|k}^a = A_d^a \hat{Z}_{k|k}^a + B_d^a v_k^a \\ P_{k+1|k} = A_d^a P_{k|k} A_d^{aT} + Q_k \\ K_k = P_{k|k-1} C_d^{aT} \left(C_d^a P_{k|k-1}^{-1} C_d^{aT} + R_k \right)^{-1} \\ \hat{Z}_{k|k}^a = \hat{Z}_{k|k-1}^a + K_k \left(Y_k - C_d^a \hat{Z}_{k|k-1}^a \right) \\ P_{k|k} = [I - K_k C_d^a] P_{k|k-1} \end{cases} \quad (13)$$

where Q_k is the covariance matrix of the process noise W_k^a , R_k is the covariance matrix of the measurement noise V_k , $\hat{Z}_{k|k}^a$ is the estimation of the extended state Z_k^a , $\hat{Z}_{k+1|k}^a$ is the estimation of the extended state Z_{k+1}^a , $P_{k|k}$ is the estimation of the covariance matrix P_k , and $P_{k+1|k}$ is the estimation of the covariance matrix P_{k+1} . Thus, we can get both the estimations of the modeling errors \hat{f}_k and the actual state $\hat{\tilde{Z}}_k$ from $\hat{Z}_{k+1|k}^a = (\hat{\tilde{Z}}_k, \hat{f}_k)$ of (13).

C. COMPENSATION CONTROL

A compensation control can be designed while using the estimated modeling errors to improve control performance of SMA actuators. In this paper, we proposed to use the state feedback control (SFC), i.e.,

$$v = -K \mathbf{e} \quad (14)$$

where $K = [k_1 \ k_2 \ k_3]$ is designed such that $A_c - B_c K$ is Hurwitz; $\mathbf{e} = [z_1 - r_d \ z_2 - \dot{r}_d \ z_3 - \ddot{r}_d]^T$ is the error vector; r_d is the reference trajectory; and z_1 , z_2 , and z_3 are the states of the reference model.

According to (9), the actual control u of the SFC can be obtained:

$$u = \alpha(\mathbf{x}) + \gamma^{-1}(\mathbf{x}) v \quad (15)$$

where $\gamma^{-1}(\mathbf{x})$ is the inverse of the matrix $\gamma(\mathbf{x})$.

For compensation control, the active updated states and modeling errors were used to calculate the control. According to (9) and (11), the control law of the proposed control is given as:

$$v = -K \tilde{\mathbf{e}} \quad (16)$$

$$u = \hat{\alpha}(\mathbf{x}) + \hat{\gamma}^{-1}(\mathbf{x}) (v + \hat{f}_3) \quad (17)$$

where $\tilde{\mathbf{e}} = [\tilde{z}_1 - r_d \ \tilde{z}_2 - \dot{r}_d \ \tilde{z}_3 - \ddot{r}_d]^T$ is the error vector; and \tilde{z}_1 , \tilde{z}_2 , and \tilde{z}_3 are the states of the active model; \hat{f}_3 is the estimation of f_3 ; $\hat{\alpha}(\mathbf{x})$ and $\hat{\gamma}(\mathbf{x})$ are the estimation of $\alpha(\mathbf{x})$ and $\gamma(\mathbf{x})$, respectively, which are updated actively with the states of the active model.

IV. EXPERIMENTAL STUDIES

Experiments were conducted to verify the performance of the proposed active modeling and control scheme.

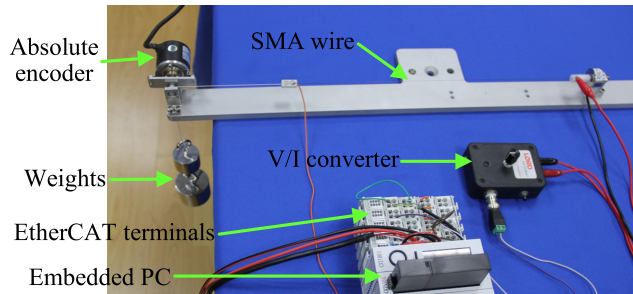


FIGURE 3. Photo of the experimental setup.

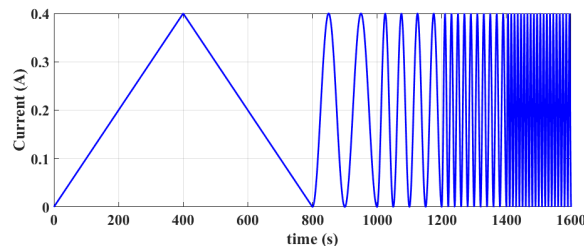


FIGURE 4. The multi-frequency current signals for identification experiment.

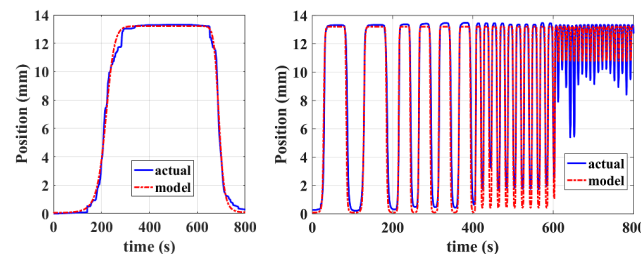


FIGURE 5. Result of position comparison between the model output and real measurement; left: Low-frequency domain, right: High-frequency domain; solid blue: Measurement, dotted red: Model output.

Shown in Fig. 3, the experimental setup consists of a SMA wire, an absolute encoder, a V/I (voltage to current) converter, and payload weights. The SMA wire we used is the Nitinol Flexinol™ wire, manufactured by Dynalloy, Inc., with 340mm length and 0.25mm diameter. The V/I converter of Wonder Box Device Controller Kit (LORD, RD-3002-03) was used to electrically heat the wire. The wire displacement was measured by the absolute encoder of CHA38B10-12B-G24RS232. The controller was built on Beckhoff TwinCAT 3, and the sampling time was set to 5ms in all the experiments in this paper.

A. MODEL IDENTIFICATION AND MODEL ERROR

In order to identify the parameters of the nonlinear SMA dynamic model of (2-6), the multi-frequency current signals, shown in Fig. 4, were designed. And the identification experiment were carried out in two phases. In the first step, the 1/800Hz triangle-wave current signal was applied on the SMA wire to obtain the quasi-static response for the estimation of the static parameters, including the phase

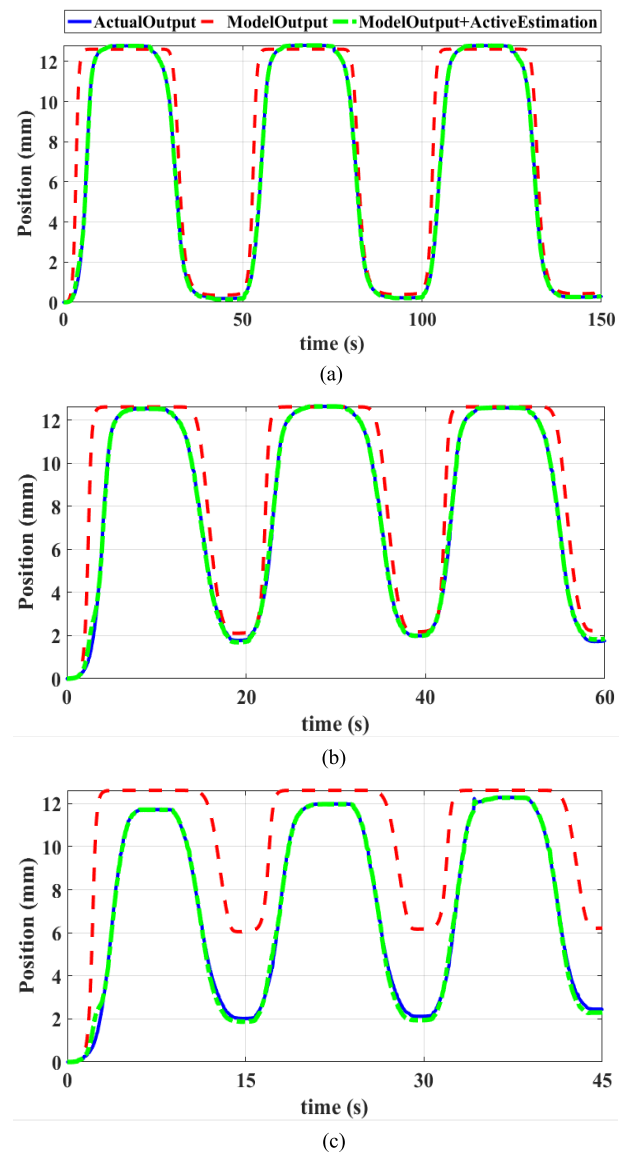


FIGURE 6. Comparisons among the actual measurement (solid blue), the model output (dashed red), and the ModelOutput+ ActiveEstimation (dash-dotted green) at three frequencies of (a) 1/50Hz, (b) 1/20Hz, and (c) 1/15Hz.

transition temperature parameters A_s, A_f, M_s, M_f , and the heat convection coefficient h_c . In the second phase, the sinusoidal signals under the frequencies of 1/100Hz, 1/50Hz, 1/20Hz, and 1/10Hz were sequentially applied on the SMA wire to excite the dynamic response for the estimation of the dynamic parameters, including the specific heat c_p , the damping coefficient c , and the inertia I .

Here the cost function was firstly defined as:

$$Err_{est} = \sum (x - x_{est})^2 \quad (18)$$

where x and x_{est} are the position measured by the encoder and that from the model calculation, respectively.

When the input current and the output position signals were acquired, the Levenberg-Marquardt algorithm (LMA),

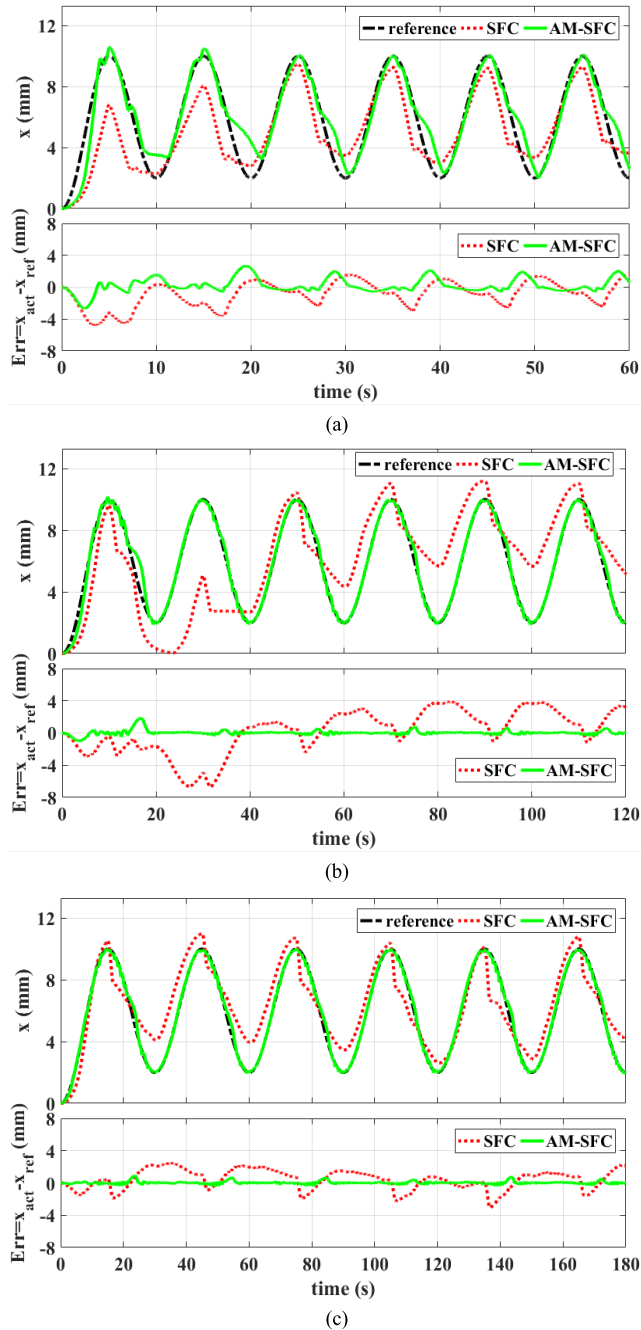


FIGURE 7. Position tracking (top in each figure) and the corresponding error (bottom) controlled by SFC and AM-SFC for sinusoidal trajectories at three different frequencies of (a) 1/10Hz, (b) 1/20Hz, and (c) 1/30Hz.

which is often used to solve nonlinear least squares problems and can be called from MATLAB/Simulink toolbox, was adopted to minimize the cost function Err_{est} of (18). The LMA interpolates between the Gauss-Newton algorithm and the method of gradient descent by adjusting a damping factor adaptively in iterative process. If the reduction of Err_{est} is rapid, a smaller value of the factor can be used, bringing the algorithm closer to Gauss-Newton algorithm to converge quickly to the optimal solution; whereas if the reduction of

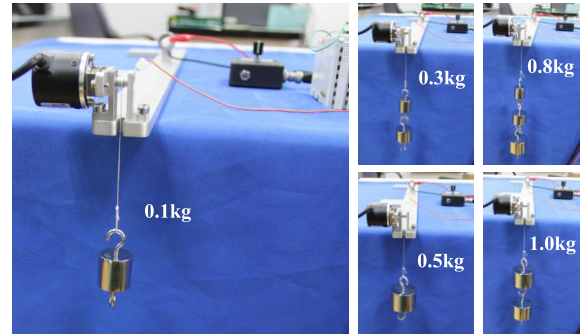


FIGURE 8. Five different loads (from left to right: 0.1kg, 0.3kg, 0.5kg, 0.8kg, 1.0kg) applied on the SMA wire.

Err_{est} is slow, the value can be increased, bringing it closer to the method of gradient descent to find a global minimum. After the two-step identification by using the LMA method, the parameters of the nonlinear SMA model were finally obtained: $A_s = 84.864$, $A_f = 144.02$, $M_s = 59.692$, $M_f = 41.891$, $h_c = 19.815$, $c_p = 102.9$, $c = 100.02$, and $I = 0.5$.

Substituting these obtained parameters into (6), we obtain the identified SMA model as:

$$\dot{\mathbf{x}} = a(\mathbf{x}) + b(\mathbf{x}) u \quad (19)$$

where

$$a(x) = \begin{bmatrix} -0.48x_1 \\ x_3 \\ -200.04x_3 + (0.08 - 2x_2) K(\xi) - 9.8 \end{bmatrix},$$

$$b(x) = \begin{bmatrix} 567.85 \\ 0 \\ 0 \end{bmatrix}.$$

Fig. 5 shows the comparison between the model output of (19) and the real measurement. We can see that the identified model presents the SMA behavior well in low frequency domain, but it becomes worse and worse as the frequency increases. This indicates that the fixed parameter model cannot describe the SMA behavior well in the whole frequency range due to strong nonlinearity, hysteresis and time-varying characteristics of SMA dynamics.

B. ACTIVE ESTIMATION OF MODELING ERRORS

The modeling errors were introduced into the linear state-space model as the extended state of (12), and we used the Kalman filter of (13) to synchronously estimate the system states and the modeling errors in real-time. The modeling errors estimated actively were used to compensate the reference model output. In order to demonstrate quantitatively the role of active estimation, we define the following index:

$$Err_{model/estm} = \frac{1}{N} \sum_{i=1}^N |x_{model/estm}^i - x_{actual}^i| \quad (20)$$

where x_{actual} indicates the real output measured by the encoder; the subscript $model$ indicates the output calculated

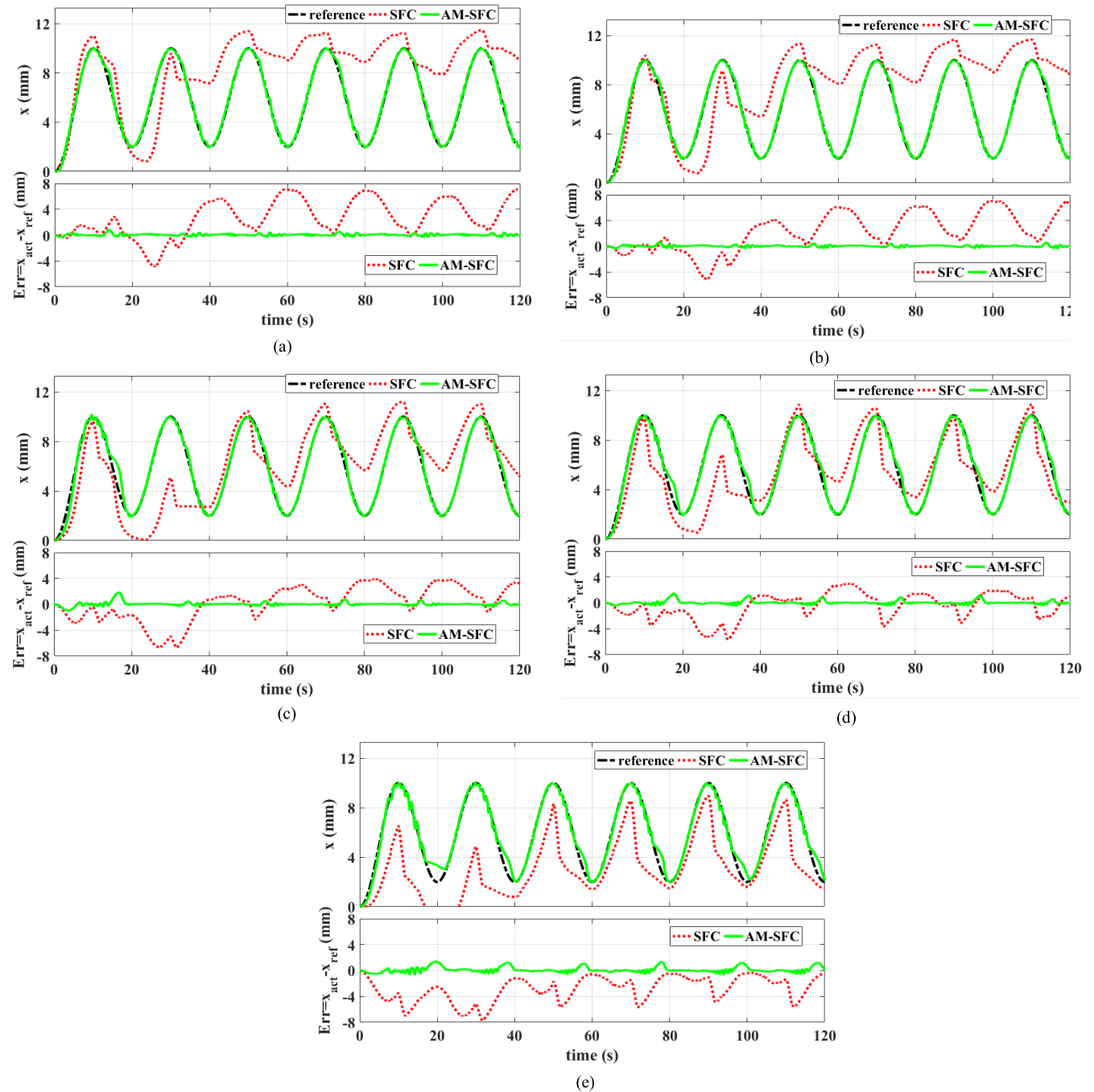


FIGURE 9. Position tracking (top in each figure) and the corresponding error (bottom) controlled by SFC and AM-SFC for tracking a 1/20Hz sinusoidal trajectory under the five different loads of (a) 0.1kg, (b) 0.3kg, (c) 0.5kg, (d) 0.8kg, and (e) 1.0kg.

by the reference model, and the subscript $estm$ represents that calculated by the reference model plus the estimated modeling errors; and N is the number of sampling points. The experiments were conducted with respect to the sinusoidal input current signals at three different frequencies, of 1/50Hz, 1/20Hz and 1/15Hz. And Fig. 6 shows the result, from which we can see that, compared to ModelOutput, ModelOutput+ActiveEstimation meets the encoder measurement much better with respect to all of the three frequencies.

Table 1 presents the index of (20) with respect to the three frequencies, which further demonstrates that the active estimation reduced more than 96% of the model error.

C. ACTIVE MODEL BASED CONTROL

The gain parameters of the state feedback control (SFC) were manually adjusted many times until achieving a satisfactory tradeoff between tracking precision and control input. And the gain vector of the SFC was finally determined as:

TABLE 1. $Err_{model/estm}$ of Fig. 6.

	Err_{model}	Err_{estm}	Reduced ($1 - Err_{estm}/Err_{model}$)
(a)	0.9608	0.0208	97.84%
(b)	1.1939	0.0405	96.61%
(c)	3.1653	0.0828	97.38%

TABLE 2. Err_{track} of Fig. 7.

	Err_{track} of SFC	Err_{track} of AM-SFC	Reduced
(a)	1.357	0.563	58.49%
(b)	2.198	0.155	92.94%
(c)	1.280	0.105	91.83%

$K = [8000 \ 500 \ 160]$. To conduct a fair comparison, the SFC gain of the proposed active model based SFC (AM-SFC) remained the same as that of the conventional SFC.

Two groups of experiments were carried out to demonstrate the improvement of the proposed AM-SFC comparing to the conventional SFC. One group was to test the tracking performance of the controller with respect to different frequency trajectories, and the other one was to check the adaptive capability of the controller with respect to different loads.

The tracking errors for the two groups of experiments were calculated as

$$Err_{track} = \frac{1}{N} \sum_{i=1}^N |x_{act}^i - x_{ref}^i| \quad (21)$$

where x_{ref} and x_{act} are the desired reference trajectory and the actual position measured by the encoder, respectively; N is the number of sampling points.

For the first group of experiments, sinusoidal trajectories at three different frequencies, i.e., $f = 1/10\text{Hz}$, $1/20\text{Hz}$, and $1/30\text{Hz}$ in (22) were set as the reference trajectories.

The tracking errors for the two groups of experiments were calculated as

$$x_{ref} = 4 \sin(2\pi f - \pi/2) + 6 \quad (22)$$

where x_{ref} is the reference trajectory, f is the frequency.

The load was fixed to 0.5kg . The performance of the SMA actuated system under the SFC and the AM-SFC is shown in Fig. 7, where the black dash-dotted curves represent the manually given reference trajectories, the red dotted curves represents the tracking results under SFC, and the green solid curves represent the tracking results under AM-SFC. From Fig. 7 we can see that the tracking errors of the proposed AM-SFC have been significantly reduced while comparing to that of the conventional SFC. Table 2 further shows the improvements in quantification. The tracking errors were reduced more than 58% by the active-model-based compensation control, while comparing to those by the normal control only. The tracking errors of AM-SFC became larger as the frequency increased. This result is corresponding with

TABLE 3. Err_{track} of Fig. 9.

	Err_{track} of SFC	Err_{track} of AM-SFC	Reduced
(a)	3.563	0.126	96.46%
(b)	3.336	0.108	96.76%
(c)	2.198	0.155	92.94%
(d)	1.567	0.167	89.34%
(e)	2.477	0.270	89.10%

the model error in Fig. 5. We can see that when $f = 1/10\text{Hz}$ the model error of the identified SMA model in Fig. 5 is poor, and the tracking error of AM-SFC in Fig. 7(a) is poor as well. Hence, the poor control performance in high frequency domain is mainly related to the low model accuracy in high frequency domain.

For the second group of experiments, shown as Fig. 8, five different loads, i.e., 0.1kg , 0.3kg , 0.5kg , 0.8kg , and 1.0kg , were sequentially applied to the SMA wire. The frequency of the reference trajectory was fixed at $f = 1/20\text{Hz}$ in (22). The SFC gain parameters remained the same with those of the first group experiments.

The performances of the SMA wire under the SFC and AM-SFC are shown in Fig. 9, from which we can see that the tracking performance of AM-SFC has been significantly improved under the five different loads while comparing to that of SFC. Table 3 further shows that the Err_{track} of (21) has been reduced by more than 89% for all of the five loads.

V. CONCLUSION

In this paper, an active model based control scheme was proposed for SMA actuators, which intended to compensate the modeling errors and improve control performance. Extensive experiments were conducted on a one-DOF SMA testbed, and the experimental results demonstrated the improvement of the proposed scheme with respect to different frequency trajectories and different loads. Compared to the conventional SFC, the proposed AM-SFC has reduced the absolute tracking error by more than 58% with respect to the three different frequency trajectories, and by more than 89% with respect to the five different loads.

In future work, the proposed method will be further improved, for example, a nonlinear estimator can be directly used to handle complex the nonlinear model of SMA actuated system, rather than taking a lot of effort to linearize the model first. Moreover, the proposed method will be applied to control SMA-actuated robots, such as bionic prosthesis and wearable exoskeleton, etc.

REFERENCES

- [1] D. Hwang, Y. S. Ihn, and K. Kim, "Compact modular cycloidal motor with embedded shape memory alloy wires," *IEEE Trans. Ind. Electron.*, vol. 65, no. 5, pp. 4028–4038, May 2018.
- [2] R. Barretta, S. A. Faghidian, and F. M. de Sciarra, "Stress-driven nonlocal integral elasticity for axisymmetric nano-plates," *Int. J. Eng. Sci.*, vol. 136, pp. 38–52, Mar. 2019.

- [3] A. Apuzzo, R. Barretta, S. A. Faghidian, R. Luciano, and F. M. de Sciarra, "Free vibrations of elastic beams by modified nonlocal strain gradient theory," *Int. J. Eng. Sci.*, vol. 133, pp. 99–108, Dec. 2018.
- [4] H. Yang, M. Xu, W. Li, and S. Zhang, "Design and implementation of a soft robotic arm driven by SMA coils," *IEEE Trans. Ind. Electron.*, vol. 66, no. 8, pp. 6108–6116, Aug. 2019.
- [5] Y. Fei and H. Xu, "Modeling and motion control of a soft robot," *IEEE Trans. Ind. Electron.*, vol. 64, no. 2, pp. 1737–1742, Feb. 2019.
- [6] C. Cheng, J. Cheng, and W. Huang, "Design and development of a novel SMA actuated multi-DOF soft robot," *IEEE Access*, vol. 7, pp. 75073–75080, 2019.
- [7] D. Copaci, F. Martín, L. Moreno, and D. Blanco, "SMA based elbow exoskeleton for rehabilitation therapy and patient evaluation," *IEEE Access*, vol. 7, pp. 31473–31484, 2019.
- [8] P. Motzki, F. Khelfa, M. Schmidt, S. Seelecke, and L. Zimmer, "Design and validation of a reconfigurable robotic end-effector based on shape memory alloys," *IEEE/ASME Trans. Mechatronics*, vol. 24, no. 1, pp. 293–303, Feb. 2019.
- [9] M. Jin, J. Lee, and K. K. Ahn, "Continuous nonsingular terminal sliding-mode control of shape memory alloy actuators using time delay estimation," *IEEE/ASME Trans. Mechatronics*, vol. 20, no. 2, pp. 899–909, Apr. 2015.
- [10] Y. Pan, Z. Guo, X. Li, and H. Yu, "Output-feedback adaptive neural control of a compliant differential SMA actuator," *IEEE Trans. Control Syst. Technol.*, vol. 25, no. 6, pp. 2202–2210, Nov. 2017.
- [11] K. K. Ahn and N. B. Kha, "Internal model control for shape memory alloy actuators using fuzzy based Preisach model," *Sens. Actuators A, Phys.*, vol. 136, no. 2, pp. 730–741, 2007.
- [12] B. K. Nguyen and K. K. Ahn, "Feedforward control of shape memory alloy actuators using fuzzy-based inverse Preisach model," *IEEE Trans. Control Syst. Technol.*, vol. 17, no. 2, pp. 434–441, Mar. 2009.
- [13] M. A. Krasnosel'skii and A. V. Pokrovskii, *Systems With Hysteresis*. New York, NY, USA: Springer-Verlag, 1989.
- [14] H. Sayyaadi and M. R. Zakerzadeh, "Position control of shape memory alloy actuator based on the generalized Prandtl-Ishlinskii inverse model," *Mechatronics*, vol. 22, no. 7, pp. 945–957, Oct. 2012.
- [15] N. T. Tai and K. K. Ahn, "A hysteresis functional link artificial neural network for identification and model predictive control of SMA actuator," *J. Process Control*, vol. 22, no. 4, pp. 766–777, Apr. 2012.
- [16] M. Brokate and J. Sprekels, "Hysteresis and phase transitions," *Appl. Math. Sci.*, vol. 121, no. 3, pp. 1325–1327, 1996.
- [17] N. T. Tai and K. K. Ahn, "Adaptive proportional–integral–derivative tuning sliding mode control for a shape memory alloy actuator," *Smart Mater. Struct.*, vol. 20, no. 5, pp. 1–13, 2011.
- [18] Y.-K. Wen, "Method for random vibration of hysteretic systems," *J. Eng. Mech. Division*, vol. 102, no. 2, pp. 249–263, 1976.
- [19] M. H. Elahinia and H. Ashrafioun, "Nonlinear control of a shape memory alloy actuated manipulator," *J. Vib. Acoust.*, vol. 124, no. 4, pp. 566–575, Oct. 2002.
- [20] G. Gilardi, E. Haslam, V. Bundhoo, and E. J. Park, "A shape memory alloy based tendon-driven actuation system for biomimetic artificial fingers, part II: Modelling and control," *Robotica*, vol. 28, no. 5, pp. 675–687, 2010.
- [21] J. Jayender, R. V. Patel, S. Nikumb, and M. Ostojević, "Modeling and control of shape memory alloy actuators," *IEEE Trans. Control Syst. Technol.*, vol. 16, no. 2, pp. 279–287, Mar. 2008.
- [22] R. Romano and E. A. Tannuri, "Modeling, control and experimental validation of a novel actuator based on shape memory alloys," *Mechatronics*, vol. 19, no. 7, pp. 1169–1177, 2009.
- [23] E. Asua, V. Etxebarria, and A. García-Arribas, "Neural network-based micropositioning control of smart shape memory alloy actuators," *Eng. Appl. Artif. Intell.*, vol. 21, no. 5, pp. 796–804, Aug. 2008.
- [24] J. C. Hannen, J. H. Crews, and G. D. Buckner, "Indirect intelligent sliding mode control of a shape memory alloy actuated flexible beam using hysteretic recurrent neural networks," *Smart Mater. Struct.*, vol. 21, no. 8, Aug. 2012, Art. no. 085015.
- [25] J. H. Wiest and G. D. Buckner, "Indirect intelligent sliding mode control of antagonistic shape memory alloy actuators using hysteretic recurrent neural networks," *IEEE Trans. Control Syst. Technol.*, vol. 22, no. 3, pp. 921–929, May 2014.
- [26] A. Kumagai, T.-I. Liu, and P. Hozian, "Control of shape memory alloy actuators with a neuro-fuzzy feedforward model element," *J. Intell. Manuf.*, vol. 17, no. 1, pp. 45–56, Feb. 2006.
- [27] K. K. Ahn and N. B. Kha, "Position control of shape memory alloy actuators using self tuning fuzzy PID controller," *Int. J. Control Autom. Syst.*, vol. 4, pp. 756–762, Dec. 2006.
- [28] S. S. Nakshatharan, K. Dhanalakshmi, and D. J. S. Ruth, "Fuzzy based sliding surface for shape memory alloy wire actuated classical super-articulated control system," *Appl. Soft Comput.*, vol. 32, no. 1, pp. 580–589, 2015.
- [29] N. T. Tai and K. K. Ahn, "A RBF neural network sliding mode controller for SMA actuator," *Int. J. Control Autom. Syst.*, vol. 8, no. 6, pp. 1296–1305, 2010.
- [30] N. T. Tai and K. K. Ahn, "Output feedback direct adaptive controller for a SMA actuator with a Kalman filter," *IEEE Trans. Control Syst. Technol.*, vol. 20, no. 4, pp. 1081–1091, Jul. 2012.
- [31] M. R. Zakerzadeh and H. Sayyaadi, "Precise position control of shape memory alloy actuator using inverse hysteresis model and model reference adaptive control system," *Mechatronics*, vol. 23, pp. 1150–1162, Dec. 2013.
- [32] B. Zhang, X.-G. Zhao, X.-G. Li, and D.-H. Zhang, "Robust indirect adaptive control for a class of nonlinear systems and its application to shape memory alloy actuators," *IEEE Access*, vol. 6, pp. 35809–35823, 2018.
- [33] N. Nikdel, P. Nikdel, M. A. Badamchizadeh, and I. Hassanzadeh, "Using neural network model predictive control for controlling shape memory alloy-based manipulator," *IEEE Trans. Ind. Electron.*, vol. 61, no. 3, pp. 1394–1401, Mar. 2014.
- [34] A. U. Awan, J. Park, J. Ryu, M. Cho, and H. J. Kim, "Adaptive control of a shape memory alloy actuator using neural-network feedforward and RISE feedback," *Int. J. Precis. Eng. Manuf.*, vol. 17, no. 4, pp. 409–418, 2016.
- [35] A. Gómez-Espinosa, R. C. Sundin, E. Cuan-Urquiza, C. D. Treviño-Quintanilla, and I. L. Eguren, "Neural network direct control with online learning for shape memory alloy manipulators," *Sensors*, vol. 19, no. 11, p. 2576, 2019.
- [36] K. Ikuta, M. Tsukamoto, and S. Hirose, "Mathematical model and experimental verification of shape memory alloy for designing micro actuator," in *Proc. IEEE Micro Electro Mech. Syst.*, Jan. 1991, pp. 103–108.
- [37] H. K. Khalil, *Nonlinear Systems*, 3rd ed. Upper Saddle River, NJ, USA: Prentice-Hall, 2002.
- [38] D. Zhang, X. Zhao, and J. Han, "Active model-based control for pneumatic artificial muscle," *IEEE Trans. Ind. Electron.*, vol. 64, no. 2, pp. 1686–1695, Feb. 2017.
- [39] P. Abbeel, A. Coates, and A. Y. Ng, "Autonomous helicopter aerobatics through apprenticeship learning," *Int. J. Robot. Res.*, vol. 29, no. 13, pp. 1–31, 2010.



DAOHUI ZHANG was born in Anhui, China, in 1986. He received the B.E. degree in mechanical engineering and automation from Northeastern University, Shenyang, China, in 2010, and the Ph.D. degree in pattern recognition and intelligent system from the Shenyang Institute of Automation, Chinese Academy of Sciences, Shenyang, in 2018.

He is currently an Associate Professor with the State Key Laboratory of Robotics, Shenyang Institute of Automation, Chinese Academy of Sciences. His main research interests include nonlinear estimation and control, robotics, and pattern recognition.



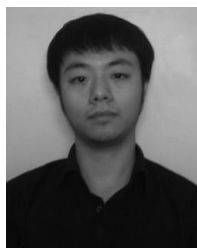
XINGANG ZHAO (M'12) was born in Shandong, China, in 1978. He received the B.E. and M.E. degrees in mechanics from Jilin University, Changchun, China, in 2000 and 2004, respectively, and the Ph.D. degree in pattern recognition and intelligent systems from the Chinese Academy of Sciences, Shenyang, China, in 2008.

From 2015 to 2016, he was a Visiting Scientist with the Rehabilitation Institute of Chicago, Chicago, USA. He is currently a Professor with the State Key Laboratory of Robotics, Shenyang Institute of Automation, Chinese Academy of Sciences. His main research interests include medical robots, rehabilitation robots, robot control, and pattern recognition.



JIANDA HAN (M'05) was born in Liaoning, China, in 1968. He received the Ph.D. degree from the Harbin Institute of Technology, Harbin, China, in 1998.

From 1998 to 2003, he was a Visiting Scientist with the City University of Hong Kong, Hong Kong; Michigan State University, East Lansing, MI, USA; and Cornell University, Ithaca, NY, USA. Since 1998, he has been with the State Key Laboratory of Robotics, Shenyang Institute of Automation, Chinese Academy of Sciences. He is currently a Professor with the College of Computer and Control Engineering, Nankai University. His research interests include nonlinear estimation and control, robotics, and mechatronics systems.



BI ZHANG was born in Liaoning, China, in 1990. He received the B.E. and Ph.D. degrees in control theories and control applications from Northeastern University, Shenyang, China, in 2012 and 2017, respectively. He is currently an Assistant Professor with the State Key Laboratory of Robotics, Shenyang Institute of Automation, Chinese Academy of Sciences. His recent research interest includes advanced control theories and their applications in rehabilitation robots.



XIAOGUANG LI was born in Liaoning, China, in 1979. She received the B.E. degree in mechanical design, manufacturing, and automation and the M.E. degree in mechanical manufacturing and automation from the Liaoning University of Technology, Jinzhou, China, in 2003 and 2006, respectively. She is currently pursuing the Ph.D. degree with the State Key Laboratory of Robotics, Shenyang Institute of Automation, Chinese Academy of Sciences. She is also a Lecturer with the Shenyang University of Technology, China. Her recent research interest includes modeling and control of smart actuator systems.